

TABLE OF CONTENTS

	Page
ACKNOWLEDGEMENTS	iii
ABSTRACT (ENGLISH)	v
ABSTRACT (THAI)	viii
LIST OF TABLES	xvi
LIST OF FIGURES	xvii
ABBREVIATION AND SYMBOLS	xxv
CHAPTER 1 INTRODUCTION	1
1.1 Overview	1
1.2 Objectives of this work	3
CHAPTER 2 LITERTURE REVIEW	4
2.1 Dielectric properties	4
2.1.1 Dielectric constant	4
2.1.2 Dielectric loss	6
2.1.3 Frequency dependence of dielectric polarization	7
2.1.4 Diffuse phase transition	8
2.2 Ferroelectric properties	10

2.2.1	Ferroelectric phases and domains	10
2.2.2	Polarization switching and hysteresis loop	12
2.2.3	Hysteresis loop slope and area	14
2.3	Thermal expansion	15
2.3.1	Thermal expansion coefficient	15
2.3.2	Thermal strain	15
2.4	Lead-free perovskite materials	16
2.4.1	Bismuth sodium titanate (BNT)	16
2.4.2	Bismuth sodium zirconate (BNZ)	19
2.4.3	Bismuth sodium zirconate titanate (BNZT)	20
CHEPTER 3 EXPERIMENTAL PROCEDURES		25
3.1	Sample preparation	25
3.1.1	Powder preparation	25
3.1.1.1	BNZ system	26
3.1.1.2	BNZT system	31
3.1.2	Ceramic fabrication	33
3.1.2.1	BNZ system	33
3.1.2.1.1	Solid state sintering	34
3.1.2.1.2	Sintering aids	39
3.1.2.2	BNZT system	41
3.2	Sample characterization	43
3.2.1	Thermal analysis	43
3.2.2	Phase analysis	44

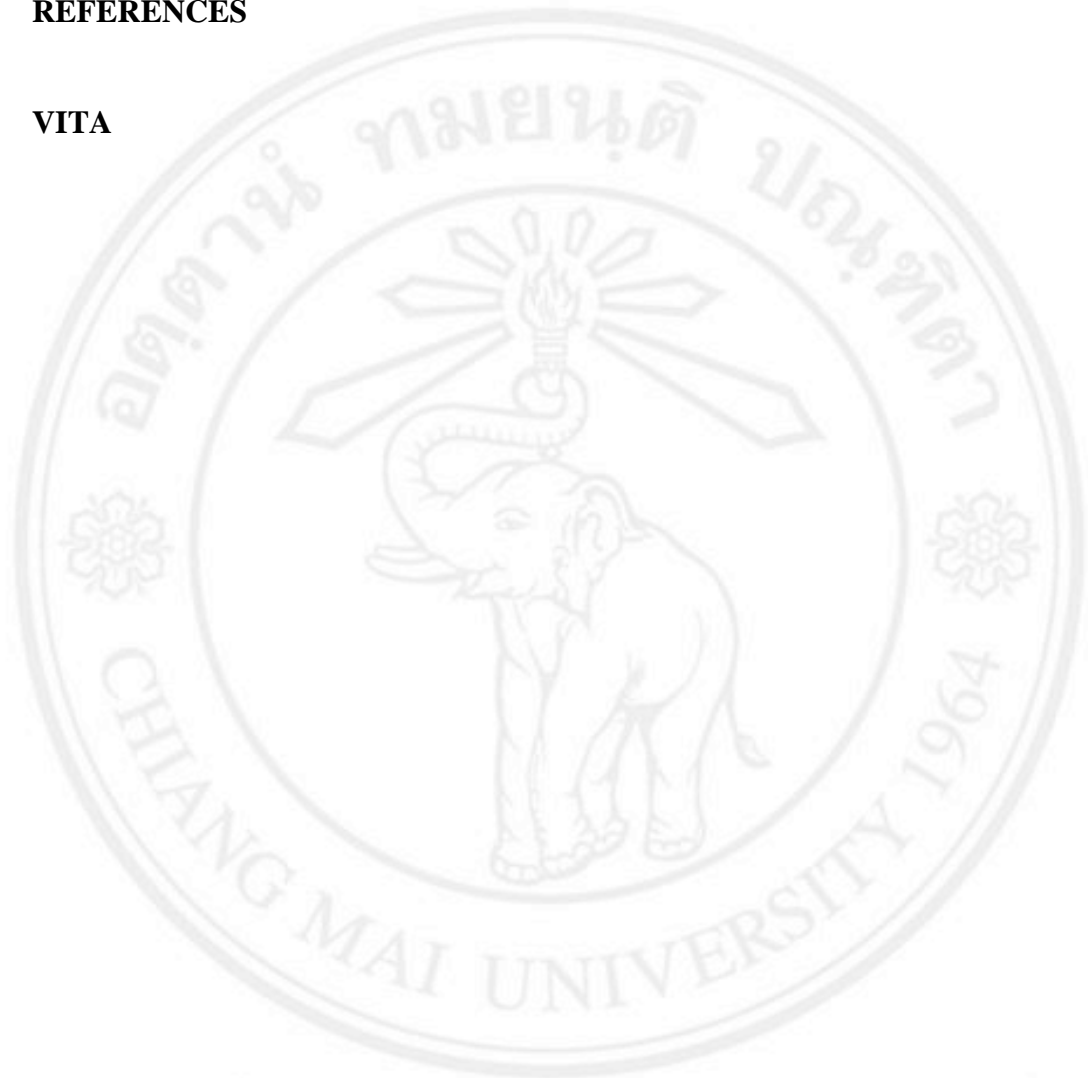
3.2.3 Crystal structure analysis	46
3.2.4 Densification analysis	47
3.2.5 Microstructural analysis	47
3.2.6 Mechanical property analysis	49
3.2.6.1 Vickers hardness	49
3.2.6.2 Knoop hardness	50
3.2.7 Thermal expansion property analysis	51
3.2.8 Dielectric property analysis	52
3.2.9 Electrical conduction analysis	54
3.2.10 Ferroelectric property analysis	56
CHEPTER 4 RESULTS AND DISCUSSION (PART I):	59
PREPARATION AND CHARACTERISTICS OF BNZ SYSTEM	
4.1 BNZ powder preparation	59
4.1.1 TG-DSC analysis	60
4.1.2 Effects of calcination temperature	61
4.1.3 Effects of calcination time	62
4.1.4 Effects of excess starting powders	63
4.2 BNZ powder morphology and chemical composition	66
4.3 BNZ crystal structure investigation	67
4.4 BNZ ceramic fabrication	68
4.4.1 Effect of sintering temperature	69
4.4.2 Effect of sintering time	74
4.4.3 Effect of initial particle characteristic	77

4.4.4 Effect of sintering aids	88
CHAPTER 5 RESULTS AND DISCUSSION (PART II): EFFECTS OF Ti ADDITION ON CHARACTERISTICS OF BNZ AND BNZT SYSTEMS	98
5.1 BNZT powder	99
5.1.1 Phase characterization	100
5.1.2 Powder morphology	101
5.2 Ceramic fabrication	103
5.2.1 Physical properties	103
5.2.1 Phase analysis	105
5.2.2 Microstructure	108
5.3 Mechanical properties	112
5.4 Thermal expansion properties	117
5.4.1 Thermal strain	117
5.4.2 Thermal expansion coefficient	120
5.5 Dielectric properties	123
5.5.1 Dielectric properties at room temperature	123
5.5.2 Temperature dependence of dielectric properties	126
5.6 Electrical conduction properties	133
5.7 Ferroelectric properties	137
CHAPTER 6 CONCLUSIONS AND SUGGESTIONS	142
6.1 Conclusions	142

6.2 Suggestions for further works 144

REFERENCES 145

VITA 156



ลิขสิทธิ์มหาวิทยาลัยเชียงใหม่
Copyright© by Chiang Mai University
All rights reserved

LIST OF TABLES

Table	Page
3.1 Specifications of the starting materials used in this study	26
4.1 Chemical composition of BNZ powders	67
4.2 Crystal structure data of BNZ powders	68
4.3 Atomic amount of the selected areas of BNZ/7wt%Bi ₂ O ₃ ceramic	96
5.1 Tolerance factors of BNZT system	99
5.2 Lattice parameters of Bi _{0.5} Na _{0.5} Zr _{1-x} Ti _x O ₃ ceramics	107
5.3 Average grain size of BNZ and BNZT ceramics	111
5.4 Mechanical properties of BNZ and BNZT ceramics	114
5.5 Dielectric loss at several frequencies of BNZ and BNZT ceramics	125
5.6 Dielectric parameters of BNZT ceramics at frequency 10 kHz	129
5.7 Remanent polarization, coercive field and energy loss of BNZT ceramics	141

LIST OF FIGURES

Figure	Page
2.1 Phasor diagram for (a) a perfect capacitor and (b) a real capacitor	6
2.2 Several polarization processes	8
2.3 Unit cells of the four phases (a) cubic, (b) tetragonal, (c) orthorhombic and (d) rhombohedral (the dotted lines in (b), (c) and (d) indicate the original cubic cell). Arrows indicate the direction of the spontaneous polarization (P_s) in each phase	11
2.4 Schematic illustrations of 180° and 90° domain walls	11
2.5 A typical P - E hysteresis loop in ferroelectrics	13
2.6 Hysteresis loop for a lossy capacitor	13
2.7 Dielectric properties as a function of temperature of BNT ceramic	17
2.8 P - E loop of BNT ceramic	18
2.9 Thermal expansion of BNT ceramic	18
2.10 X-ray diffraction pattern of BNZ ceramic	19
2.11 Temperature dependence of real and imaginary parts of impedance of BNZ at different frequencies	20
2.12 Pseudo-Cole-Cole plot of BNZ at different frequencies	20
2.13 Zr concentration dependence of lattice parameters of $\text{Bi}_{0.5}\text{Na}_{0.5}\text{Ti}_{1-x}\text{Zr}_x\text{O}_3$ ceramics	21
2.14 Zr concentration dependence of transition temperature of $\text{Bi}_{0.5}\text{Na}_{0.5}\text{Ti}_{1-x}\text{Zr}_x\text{O}_3$ ceramics	22

2.15	Knoop hardness and Young's modulus of $\text{Bi}_{0.5}\text{Na}_{0.5}\text{Ti}_{1-x}\text{Zr}_x\text{O}_3$ ceramics	23
2.16	Temperature dependence of dielectric constant at frequency of 10 kHz for $\text{Bi}_{0.5}\text{Na}_{0.5}\text{Ti}_{1-x}\text{Zr}_x\text{O}_3$ ceramics	24
2.17	Temperature dependence of dielectric loss at frequency of 10 kHz for $\text{Bi}_{0.5}\text{Na}_{0.5}\text{Ti}_{1-x}\text{Zr}_x\text{O}_3$ ceramics	24
3.1	Diagram of calcination $\text{Bi}_{0.5}\text{Na}_{0.5}\text{ZrO}_3$ powder at different temperatures	27
3.2	Diagram showing processing sequence of $\text{Bi}_{0.5}\text{Na}_{0.5}\text{ZrO}_3$ powders	27
3.3	Diagram showing processing sequence of $\text{Bi}_{0.5}\text{Na}_{0.5}\text{ZrO}_3$ powders with addition of starting powders	29
3.4	Diagram of calcination $\text{Bi}_{0.5}\text{Na}_{0.5}\text{ZrO}_3$ powder at different times	30
3.5	Diagram showing processing sequence of $\text{Bi}_{0.5}\text{Na}_{0.5}\text{ZrO}_3$ powder with different calcination times	31
3.6	Diagram of calcination $\text{Bi}_{0.5}\text{Na}_{0.5}\text{Zr}_{1-x}\text{Ti}_x\text{O}_3$ powders	32
3.7	Diagram showing processing sequence of $\text{Bi}_{0.5}\text{Na}_{0.5}\text{Zr}_{1-x}\text{Ti}_x\text{O}_3$ powders	33
3.8	Sample arrangements for the sintering process where a = top view and b = side view	34
3.9	Diagram for sintering process of $\text{Bi}_{0.5}\text{Na}_{0.5}\text{ZrO}_3$ ceramic with different temperatures	35
3.10	Diagram showing processing sequence of $\text{Bi}_{0.5}\text{Na}_{0.5}\text{ZrO}_3$ ceramic with different temperatures	35
3.11	Diagram for sintering process of $\text{Bi}_{0.5}\text{Na}_{0.5}\text{ZrO}_3$ ceramic with different sintering times	36
3.12	Diagram showing processing sequence of $\text{Bi}_{0.5}\text{Na}_{0.5}\text{ZrO}_3$ ceramic with different sintering times	37

3.13	Diagram for sintering process of $\text{Bi}_{0.5}\text{Na}_{0.5}\text{ZrO}_3$ ceramic with different ball milling times	38
3.14	Diagram showing processing sequence of $\text{Bi}_{0.5}\text{Na}_{0.5}\text{ZrO}_3$ ceramic with different ball milling times	38
3.15	Diagram for sintering process of $\text{Bi}_{0.5}\text{Na}_{0.5}\text{ZrO}_3$ ceramic with Bi_2O_3 or Na_2CO_3 as sintering aids	39
3.16	Diagram showing processing sequence of $\text{Bi}_{0.5}\text{Na}_{0.5}\text{ZrO}_3$ ceramic using Bi_2O_3 or Na_2CO_3 as sintering aids	40
3.17	Diagram for sintering process of $\text{Bi}_{0.5}\text{Na}_{0.5}\text{Zr}_{1-x}\text{Ti}_x\text{O}_3$ ceramics	41
3.18	Diagram showing processing sequence of $\text{Bi}_{0.5}\text{Na}_{0.5}\text{Zr}_{1-x}\text{Ti}_x\text{O}_3$ ceramics	42
3.19	Q10 Differential scanning calorimeter	43
3.20	X-ray diffractometer (Model Phillips Expert)	44
3.21	Schematic diagram of Bragg's law reflection	45
3.22	Feature of Powder Cell software	46
3.23	Scanning electron microscope (SEM, JEOL JSM-6335F)	48
3.24	Sputter coater (JFC-1100E)	48
3.25	Digital Microhardness Tester	49
3.26	The thermal expansion measurement	52
3.27	The dielectric properties measurement at room temperature	53
3.28	The dielectric properties measurement at different temperature	54
3.29	The resistivity and conductivity measurements	55
3.30	Ferroelectric hysteresis loop measurement	56
4.1	TG-DSC curve of the mixed starting powders	61
4.2	X-ray diffraction patterns of BNZ powders calcined at 700-850°C	62

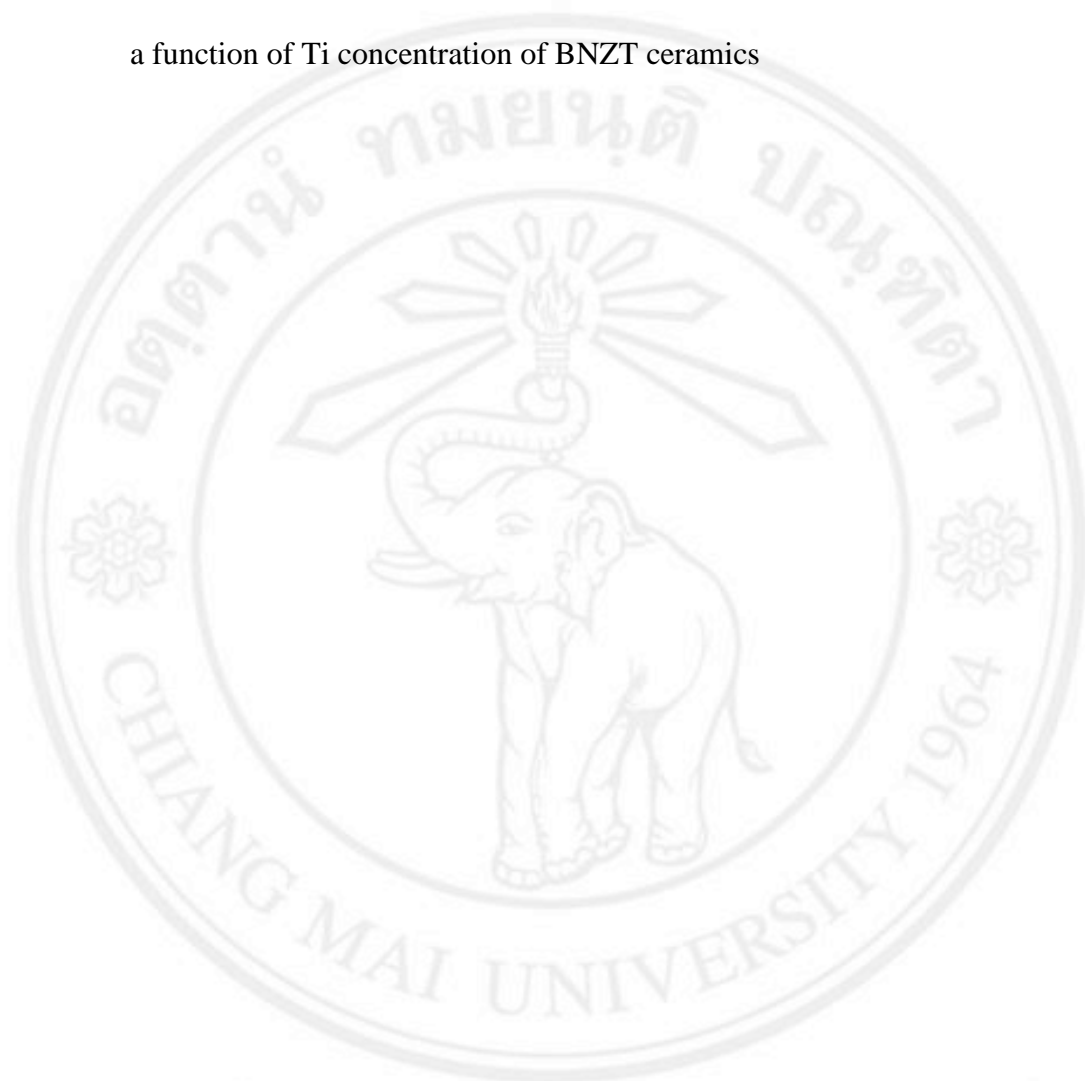
4.3	X-ray diffraction patterns of BNZ powders calcined at 800°C for 2-8 h	63
4.4	X-ray diffraction patterns of BNZ/xNa ₂ CO ₃ powders	64
4.5	X-ray diffraction patterns of BNZ/xBi ₂ O ₃ powders	65
4.6	X-ray diffraction patterns of BNZ/xZrO ₂ powders	65
4.7	BNZ powder characterization (a) powder morphology (b) particle size distribution	66
4.8	EDX analysis of BNZ powders	67
4.9	Fitting result of BNZ powders by Powder Cell Software	68
4.10	Volume shrinkage and weight loss of BNZ ceramics with different temperatures	70
4.11	XRD patterns of BNZ ceramics with different temperatures	71
4.12	SEM images of BNZ ceramics with different temperatures where a = 850, b = 900, c = 950, d = 1000, e = 1050 and f = 1100°C	73
4.13	Relative densities of BNZ ceramics with different sintering temperatures	74
4.14	Volume shrinkage and weight loss of BNZ ceramics with different time	75
4.15	XRD patterns of BNZ ceramics sintered at different sintering time	76
4.16	Relative densities of BNZ ceramics sintered at different time	77
4.17	XRD patterns of BNZ powder with different milling time	78
4.18	Lattice parameters of BNZ powder at different milling time	78
4.19	BNZ powder morphologies with different ball milling time where a = 0, b = 24, c = 48, d = 72 and e = 96 h	80
4.20	Frequency distribution of BNZ particle size with different ball milling time	81

4.21	Volume shrinkage and weight loss of BNZ ceramics with different ball milling time	83
4.22	XRD patterns of BNZ ceramics with different milling time	83
4.23	Lattice parameters of BNZ ceramics at different milling time	84
4.24	Crystallite size and microstrain of BNZ powder and ceramics at different milling time	84
4.25	SEM images of BNZ ceramics with different ball milling time where a = 0, b = 24, c = 48, d = 72 and e = 96 h	86
4.26	Frequency distribution of BNZ grain size with different ball milling time	87
4.27	Relative density as a function of ball milling time for BNZ ceramics	88
4.28	Volume shrinkage and weight loss of BNZ72/Na ₂ CO ₃ ceramics with different sintering temperatures	91
4.29	Volume shrinkage and weight loss of BNZ72/Bi ₂ O ₃ ceramics with different sintering temperatures	91
4.30	Relative densities of BNZ72/Na ₂ CO ₃ and BNZ72/Bi ₂ O ₃ ceramics with different sintering temperatures	92
4.31	XRD patterns of BNZ/xBi ₂ O ₃ ceramics sintered at 850°C	94
4.32	Lattice parameters of BNZ/xBi ₂ O ₃ ceramics sintered at 850°C	94
4.33	SEM images of BNZ/xBi ₂ O ₃ ceramics sintered at 850°C, where a = 0, b = 1, c = 4, d = 7 and e = 10 wt%	95
4.34	EDX analysis of the selected areas of BNZ/7wt%Bi ₂ O ₃ ceramic where a = gray area and b = white area	96
4.35	Frequency distribution of BNZ/Bi ₂ O ₃ grain sized ceramics sintered at 850°C	97

5.1	X-Ray diffraction patterns of BNZT powders (a) 20-80° and (b) 54-58°	101
5.2	BNZT powder morphologies with different Ti concentration where a = 0, b = 0.1, c = 0.2, d = 0.3, e = 0.4, f = 0.5 and g = 0.6	102
5.3	Volume shrinkage and weight loss of BNZT ceramics	104
5.4	Relative densities of BNZT ceramics	104
5.5	X-Ray diffraction patterns of BNZT ceramics	106
5.6	Plot of (123), (321) and (300) 2θ positions as a function of Ti concentration of BNZT ceramics	108
5.7	SEM images of BNZT ceramics where a = 0, b = 0.1, c = 0.2, d = 0.3, e = 0.4, f = 0.5 and g = 0.6	110
5.8	EDX analysis of the selected areas of BNZT ceramic x = 0.3 where a = gray area, b = dark gray area and c = white area	111
5.9	Fracture surface micrographs of BNZT ceramics where a = 0, b = 0.1, c = 0.2, d = 0.3, e = 0.4, f = 0.5 and g = 0.6	113
5.10	Knoop indentations of BNZT ceramics where a = 0, b = 0.1, c = 0.2, d = 0.3, e = 0.4, f = 0.5 and g = 0.6	115
5.11	Vickers indentations of BNZT ceramics where a = 0, b = 0.1, c = 0.2, d = 0.3, e = 0.4, f = 0.5 and g = 0.6	116
5.12	Temperature dependence of thermal strain of BNZ and BNZT ceramics for (a) x = 0, (b) x = 0.1, (c) x = 0.2, (d) x = 0.3, (e) x = 0.4, (f) x = 0.5 and (g) x = 0.6, The insets show thermal strain in heating and cooling cycles	119
5.13	Temperature dependence of polarization of BNZ and BNZT ceramics	120

5.14	Temperature dependence of thermal expansion coefficient of BNZ and BNZT ceramics for $x = 0$, (b) $x = 0.1$, (c) $x = 0.2$, (d) $x = 0.3$, (e) $x = 0.4$, (f) $x = 0.5$ and (g) $x = 0.6$	122
5.15	Dielectric constant as a function of Ti concentration of BNZ and BNZT ceramics	125
5.16	Temperature dependence of dielectric constant and loss tangent, respectively, of BNZT ceramics at different frequencies for (a) and (b) $x = 0$, (c) and (d) $x = 0.3$ and (e) and (f) $x = 0.6$	127
5.17	Temperature dependence of inverse dielectric constant $\left(\frac{1}{\epsilon_r}\right)$ for BNZT ceramics at frequency 10 kHz for (a) $x = 0$, (b) $x = 0.3$ and (c) $x = 0.6$	129
5.18	Plots of $\log\left(\frac{1}{\epsilon_r} - \frac{1}{\epsilon_m}\right)$ as a function of $\log(T - T_m)$ for BNZT ceramics at frequency 10 kHz where (a) $x = 0$, (b) $x = 0.3$ and (c) $x = 0.6$	131
5.19	Ti concentration dependence of dielectric properties of BNZT ceramics for (a) = dielectric constant and (b) = loss tangent	132
5.20	Ti concentration dependence average maximum temperatures of BNZT ceramics	133
5.21	Comparison between dc conductivity at room temperature of $\text{BNZ}_{1-x}\text{T}_x$, BNT and BNT-based ceramics	134
5.22	Plots of $\ln \sigma$ as a function of inverse temperature for BNZT ceramics at frequency 10 kHz where (a) $x = 0$, (b) $x = 0.3$ and (c) $x = 0.6$	136

5.23	<i>P-E</i> hysteresis loops of BNZT ceramics	138
5.24	Plot of the relative permittivity at high and low electric field as a function of Ti concentration of BNZT ceramics	140



ลิขสิทธิ์มหาวิทยาลัยเชียงใหม่
Copyright© by Chiang Mai University
All rights reserved

ABBREVIATIONS AND SYMBOLS

BNZ	bismuth sodium zirconate
BNT	bismuth sodium titanate
BNZT	bismuth sodium zirconate titanate
Bi	bismuth
Na	sodium
Zr	zirconate
Ti	titanate
MPB	morphotropic phase boundary
ABO ₃	perovskite structure
PVA	polyvinyl alcohol
T_c	Curie temperature
T_m	Temperature at maximum dielectric constant
XRD	X-ray diffraction
SEM	scanning electron microscope
EDX	energy dispersive X-ray
°C/min	degree Celsius per minute

λ	wavelength
χ	dielectric susceptibility
D	electric displacement
V	voltage
Q	charge
C	capacitance
ρ	bulk density
ρ_w	density of water
r	ionic radius
ϕ	diameter
t	thickness
$P-E$	polarization-electric field
α	thermal expansion coefficient
P_d	local or defect polarization
ϵ_r	material's relative permittivity (also simply called permittivity or dielectric constant)
ϵ_0	vacuum permittivity (8.85×10^{-12} F/m)

$\tan\delta$	dielectric loss or dissipation factor
σ	conductivity
E_a	activation energy
K	Boltzmann constant (1.38×10^{-23} J/K)
E_{max}	maximum electric field
E_{sw}	switching electric field
P_r	remanent polarization
P_s	spontaneous polarization
P_{max}	maximum polarization